

# A GLOBAL CLIMATOLOGY OF $\text{O}_2 \cdot \text{O}_2$ , $\text{O}_2 \cdot \text{N}_2$ , AND $(\text{H}_2\text{O})_2$ ABUNDANCE AND ABSORPTION

Charles S. Zender\* and Petr Chýlek

National Center for Atmospheric Research, Boulder, Colorado, and  
Atmospheric Science Program, Dalhousie University, Halifax, Canada

## 1. INTRODUCTION

Recent experimental and theoretical results show that the collision pairs  $\text{O}_2 \cdot \text{O}_2$  and  $\text{O}_2 \cdot \text{N}_2$  absorb a small but significant fraction of the globally incident solar radiation (Pfeilsticker et al., 1997; Solomon et al., 1998; Mlawer et al., 1998). The contribution of the water vapor dimer to shortwave absorption, however, remains speculative due to uncertainties in both its abundance and its absorption cross section (Chýlek and Geldart, 1997; Chýlek et al., 1998; Tso et al., 1998). This study employs a specially modified version of the NCAR CCM3 general circulation model to quantify the global abundances and shortwave radiative forcings of  $\text{O}_2 \cdot \text{X}$  ( $\text{O}_2 \cdot \text{X} \equiv \text{O}_2 \cdot \text{O}_2 + \text{O}_2 \cdot \text{N}_2$ ) and  $(\text{H}_2\text{O})_2$ , and the present uncertainties in these quantities.

## 2. METHODS

Quantifying the global radiative forcing of a trace gas requires good characterization of both the global abundance and the spectral absorptance of the gas. In this study, all absorber abundances were computed every timestep (20 min.) in a one year integration of the NCAR CCM3 general circulation model. Monthly gridpoint biases in the CCM simulation of pressure  $p$ , temperature  $T$ , and water vapor  $q_{\text{H}_2\text{O}}$  are generally much less than uncertainties in absorber cross-section or abundance.

The abundance of  $\text{O}_2 \cdot \text{X}$  is the product of the concentrations of  $\text{O}_2$  and X,  $[\text{O}_2]$  and  $[\text{X}]$ , respectively. CCM gridpoint errors in monthly  $[\text{O}_2]$  and  $[\text{N}_2]$  are  $< 5\%$ , and stem from biases in model  $p$ ,  $T$ , and orography. The resulting uncertainty in  $[\text{O}_2 \cdot \text{O}_2]$  and  $[\text{O}_2 \cdot \text{N}_2]$  is  $< 10\%$ .

The mass mixing ratio of  $(\text{H}_2\text{O})_2$  takes the form

$$q_{(\text{H}_2\text{O})_2} = \text{RH } q_{\text{H}_2\text{O}} a \exp(-b/T) \text{ kg kg}^{-1} \quad (1)$$

---

\*Corresponding author address: Charles S. Zender, National Center for Atmospheric Research, P.O.B. 3000, Boulder, CO 80307-3000; zender@ncar.ucar.edu

where RH is relative humidity and  $a = 144$  and  $b = 3535$  are parameters adjusted to fit experimental and *ab initio* model results (Chýlek et al., 1998). Other combinations of *ab initio* results and measurements predict  $q_{(\text{H}_2\text{O})_2}$  up to four times larger. Note that our  $q_{(\text{H}_2\text{O})_2}$  scales linearly with RH, even in clouds.

We employ  $\text{O}_2 \cdot \text{X}$  binary absorption cross-sections  $\sigma_b(\lambda)$  from Solomon et al. (1998). The uncertainty in  $\sigma_b(\lambda)$  is  $< 10\%$  for  $0.335 < \lambda < 1.137 \mu\text{m}$  (Greenblatt et al., 1990). Uncertainty in  $1.26 \mu\text{m}$  band absorption is  $\sim 30\%$  (Solomon et al., 1998; Mlawer et al., 1998). We do not include absorption in the  $1.58 \mu\text{m}$  band, which amounts to  $\sim 3\%$  of  $\text{O}_2 \cdot \text{O}_2$  absorption (Mlawer et al., 1998). The parameter  $\epsilon$  defines the efficiency of  $\text{N}_2$  relative to  $\text{O}_2$  as a partner for inducing absorption in the  $\text{O}_2$   $1.26 \mu\text{m}$  band. These previous studies show  $0.1 \leq \epsilon \leq 0.3$ , with the preponderance of studies suggesting  $\epsilon = 0.3$ . We employ  $\epsilon = 0.2$ .

Definitive laboratory measurements of  $(\text{H}_2\text{O})_2$  absorption cross-sections  $\sigma(\lambda)$  do not exist in the shortwave. We employ a  $3 \text{ cm}^{-1}$  resolution  $\sigma(\lambda)$  from an *ab initio* model (Tso et al., 1998). The uncertainty in location of individual absorption bands is  $\sim 200 \text{ cm}^{-1}$ . The large uncertainty in  $\sigma(\lambda)$  contributes an uncertainty factor of 2–4 to total  $(\text{H}_2\text{O})_2$  broadband absorption.

In the shortwave (SW), the CCM employs an 18 spectral bin  $\delta$ -Eddington approximation (Briegleb, 1992). We created  $\bar{\sigma}_i$  for the CCM SW bins by spectrally averaging  $\sigma_i(\lambda)$  from the source resolution to the CCM resolution. This procedure included weighting the high resolution cross sections by the incident solar flux at the top of the atmosphere, and, in the case of  $(\text{H}_2\text{O})_2$ , by the atmospheric transmission simulated in a more detailed 1690 band Shortwave Narrow Band (SWNB) model (Zender et al., 1997). The CCM  $\bar{\sigma}_i$  were then tuned offline until CCM and SWNB absorption agreed for each absorber in atmospheric profiles ranging from the Arctic to the Tropics.

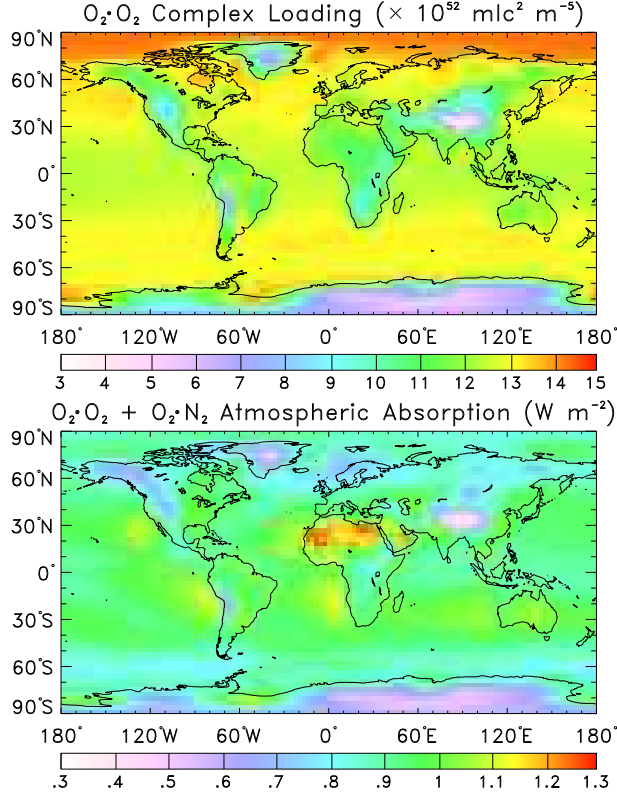


Figure 1: (a) Annual average column abundance ( $\text{mlc}^2 \text{m}^{-5}$ ) of  $\text{O}_2 \cdot \text{O}_2$ . (b) Annual average instantaneous change in atmospheric absorption ( $\text{W m}^{-2}$ ) due to  $\text{O}_2 \cdot \text{O}_2$ .

### 3. RESULTS

The modified CCM was integrated for twelve months without any radiative feedbacks from the three new absorbers.  $\text{O}_2 \cdot \text{O}_2$ ,  $\text{O}_2 \cdot \text{N}_2$ , and  $(\text{H}_2\text{O})_2$  abundances and instantaneous SW radiative forcings were diagnosed every timestep and output as monthly averages, from which the following annual averages were constructed. Except where noted the qualitative features of  $\text{O}_2 \cdot \text{N}_2$  abundance and absorption are the same as for  $\text{O}_2 \cdot \text{O}_2$ .

#### 3.1 Annual Average Abundances and Forcings

Figure 1a shows the simulated annual average column abundance of  $\text{O}_2 \cdot \text{O}_2$ . The major meridional gradient in  $\text{O}_2 \cdot \text{O}_2$  is caused by the poleward decrease in zonal average  $T$ . Arctic air is denser than tropical air, and since  $[\text{O}_2 \cdot \text{O}_2]$  depends on the square of  $[\text{O}_2]$ ,  $[\text{O}_2 \cdot \text{O}_2]$  is  $\sim 20\%$  greater in the Arctic than the Tropics at the same sea level pressure. The same would be true of the Antarctic, except the Antarctic plateau displaces the densest portion of the Tropo-

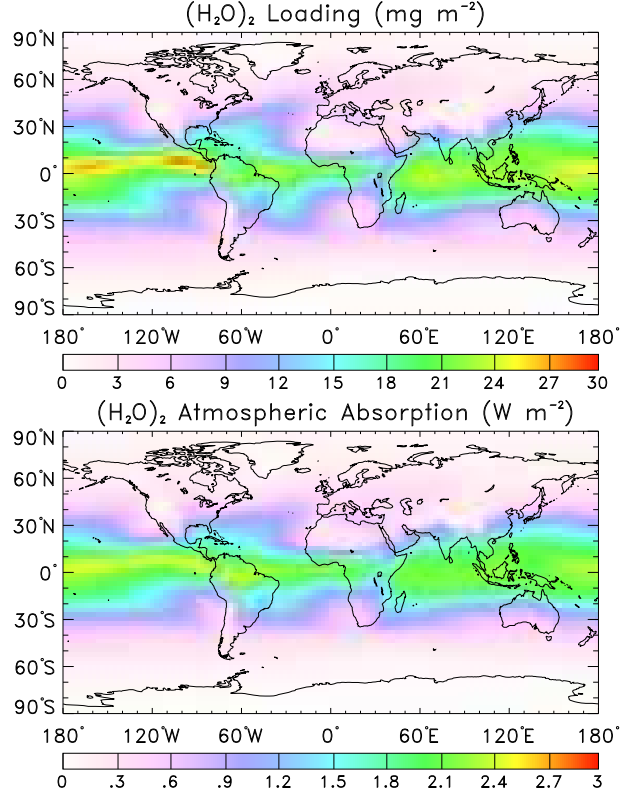


Figure 2: As in Figure 1 but for: (a)  $(\text{H}_2\text{O})_2$  abundance ( $\text{mg m}^{-2}$ ). (b) Atmospheric absorption due to  $(\text{H}_2\text{O})_2$ .

sphere, significantly reducing  $\text{O}_2 \cdot \text{O}_2$  column abundance. The Tibetan Plateau, Greenland, and the Andes also show significant orographic reduction in  $[\text{O}_2 \cdot \text{O}_2]$ . Note that orographic reduction of  $[\text{O}_2 \cdot \text{O}_2]$  is time-invariant, in contrast to effects of seasonally varying  $T$  and  $p$  in the polar regions.

Figure 1b shows the annual average SW radiative forcing of the atmosphere (increase in absorption) due to  $\text{O}_2 \cdot \text{X}$ . The annual forcing resembles the abundance, but some new features are evident. First note the enhanced atmospheric absorption above bright, low surfaces (snow, desert, stratus clouds). Since the spectral optical depth of the  $\text{O}_2 \cdot \text{O}_2$  bands is  $\lesssim 0.02$ , absorption in these bands is in the linear limit where an increase in photon path length due to reflection causes a proportionate increase in atmospheric absorption. The zonal annual average atmospheric absorption due to  $\text{O}_2 \cdot \text{X}$  is about  $0.9 \text{ W m}^{-2}$ , and is nearly invariant with latitude (not shown).

Figure 2a shows the simulated annual average column abundance of  $(\text{H}_2\text{O})_2$ . Since  $[(\text{H}_2\text{O})_2]$  depends on the square of  $[\text{H}_2\text{O}]$ , the poleward decrease in  $[(\text{H}_2\text{O})_2]$  is dictated by the square of the meridional gradient of the saturated vapor pressure  $q_s$

Absorber	Units	Abundance	Uncertainty
$O_2 \cdot O_2$	$\text{mlc}^2 \text{ cm}^{-5}$	$1.2 \times 10^{43}$	$\pm 10\%$
$O_2 \cdot N_2$	$\text{mlc}^2 \text{ cm}^{-5}$	$4.6 \times 10^{43}$	$\pm 10\%$
$(H_2O)_2$	$\text{mlc cm}^{-2}$	$1.66 \times 10^{16}$	$1-4 \times$
$(H_2O)_2$	$\text{mg m}^{-2}$	9.9	$1-4 \times$

Table 1: Global Annual Average Abundances

Forcing [ $\text{W m}^{-2}$ ]	$O_2 \cdot O_2$	$O_2 \cdot N_2$	$(H_2O)_2$
Atmospheric Absorption	0.78	0.15	0.96
(same, but for clear sky)	(0.78)	(0.17)	(1.14)
Surface Absorption	-0.42	-0.08	-0.69
Sfc. + Atm. Absorption	0.36	0.07	0.28
Surface Insolation	-0.50	-0.10	-0.76

Table 2: Global Annual Average Forcings ( $\text{W m}^{-2}$ )

in the lower troposphere.  $q_s$  varies exponentially with surface temperature, so the poleward decline in  $[(H_2O)_2]$  is quite strong. Zonal annual average  $(H_2O)_2$  absorption (not shown) in the Tropics (averaged  $20^\circ\text{S}-20^\circ\text{N}$ ) is  $1.83 \text{ W m}^{-2}$ , roughly 3.5 times greater than in the Northern Mid-latitudes (averaged  $30^\circ\text{N}-50^\circ\text{N}$ ). The ITCZ and continental centers of deep convection appear as the regions of strongest forcing.

The global average statistics for Figures 1 and 2 are summarized in Tables 1 and 2. Note that the global annual average clear sky atmospheric forcing by  $(H_2O)_2$  is predicted to exceed the cloudy sky forcing by nearly 20%. This is because all clouds except low stratus shield more  $(H_2O)_2$  beneath them from solar radiation than there is  $(H_2O)_2$  above them. Of course, if an unknown mechanism were producing more  $(H_2O)_2$  than we assume within clouds (1), this would not necessarily be the case.

### 3.2 Seasonal Patterns of Abundances and Forcings

Due to the seasonal cycle of solar insolation and the natural variability of organized tropical convection, annual average forcings alone do not suffice to characterize the geographic and vertical distribution of the forcings as they impact the climate system. As illustration we present Northern Summer (June-July-August, or JJA) seasonal average forcings.

Figure 3a shows the simulated JJA average radiative forcing of  $O_2 \cdot X$ . Most remarkable is the large polar region where atmospheric  $O_2 \cdot X$  absorption exceeds  $1.5 \text{ W m}^{-2}$ .  $O_2 \cdot X$  forcing peaks in the polar Summer, when peak solar insolation coincides with the largest  $O_2 \cdot X$  abundances (Figure 1a). Antarctic

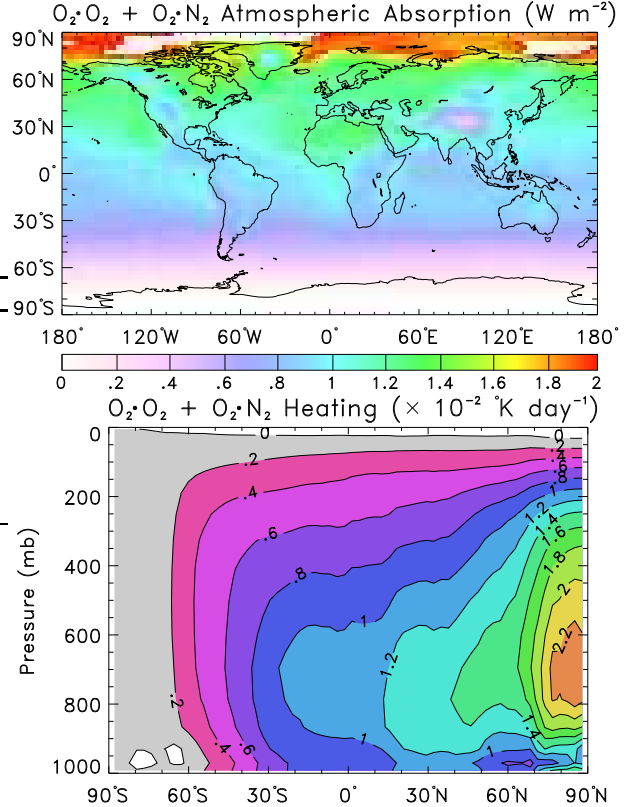


Figure 3: Seasonal average instantaneous radiative forcing in Northern Summer (JJA average) due to  $O_2 \cdot O_2 + O_2 \cdot N_2$ . (a) Atmospheric absorption ( $\text{W m}^{-2}$ ). (b) Heating rate ( $\times 10^{-02} \text{ }^\circ\text{K day}^{-1}$ )

Summer forcings (not shown) are nearly symmetric about the Equator to Figure 3. Equinoctial forcings (not shown) extend farther into the Winter Hemisphere than Solstitial forcings, and are weaker.

Figure 3b shows the vertical distribution of the simulated JJA average, zonal average, SW radiative heating due to  $O_2 \cdot X$ . Seasonal  $O_2 \cdot O_2$  heating in excess of  $0.02 \text{ }^\circ\text{K day}^{-1}$  extends throughout the Arctic troposphere. This is 2–5% of local SW heating due to all other absorbers. The heating decreases vertically due to decreasing  $[O_2 \cdot X]$ , and decreases Southward due to decreasing daylight hours. Heating in the Antarctic Summer troposphere is similar, but slightly stronger, probably due to higher surface albedo. Most GCMs have strong cold biases at the summertime polar tropopause. It is likely that allowing  $O_2 \cdot X$  radiative feedbacks will ameliorate, though not eliminate, these biases.

Figure 4a shows the simulated JJA average radiative forcing of  $(H_2O)_2$ . The Southwest Monsoon over the Indian subcontinent dominates the zonal signature of  $(H_2O)_2$  absorption, and the ITCZ also stands

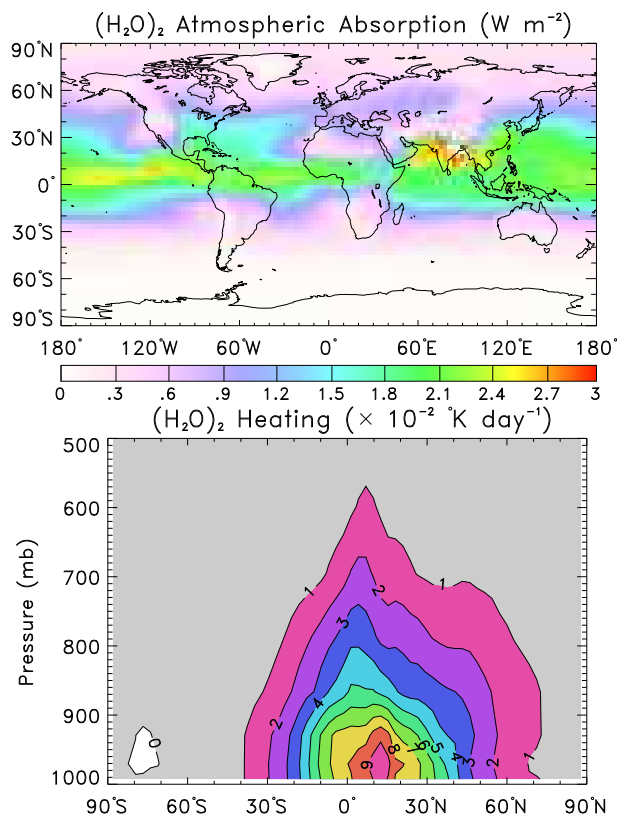


Figure 4: As in Figure 3 but for  $(\text{H}_2\text{O})_2$ .

out.  $(\text{H}_2\text{O})_2$  absorption should be most evident at the ARM CART site during this season. Figure 4b shows the concomitant  $(\text{H}_2\text{O})_2$  heating distribution. Heating due to  $(\text{H}_2\text{O})_2$  is strongest in the lower troposphere, reaching nearly  $0.1 \text{ }^\circ\text{K day}^{-1}$  in the Asian Monsoon and ITCZ regions.  $(\text{H}_2\text{O})_2$  heating reaches its greatest vertical and Northward extents during JJA. Heating during other seasons (not shown) is otherwise very similar.

#### 4. CONCLUSIONS

The global distributions of  $[\text{O}_2\cdot\text{O}_2]$  and  $[\text{O}_2\cdot\text{N}_2]$  depend most on zonal average  $T$ ,  $p$ , and orography.  $\text{O}_2\cdot\text{X}$  absorbs approximately  $0.93 \text{ W m}^{-2}$  of incident solar radiation with a strong seasonal and meridional dependence. This absorption is comparable to the anthropogenic forcing of important greenhouse gases. Because of this, and the relatively small uncertainties in  $\text{O}_2\cdot\text{X}$  abundance and cross-sections,  $\text{O}_2\cdot\text{X}$  should be implemented in GCMs.  $\text{O}_2\cdot\text{X}$  has the most potential to improve the simulated climate in summertime polar regions.

The distribution of  $(\text{H}_2\text{O})_2$  centers on regions of organized deep convection such at the ITCZ and

Monsoon regions.  $(\text{H}_2\text{O})_2$  heating is centered in the lower tropical troposphere. The absolute abundance of  $(\text{H}_2\text{O})_2$  is still poorly known, as is its absorption cross-section. Using our set of assumptions,  $(\text{H}_2\text{O})_2$  forcing is comparable to  $\text{O}_2\cdot\text{X}$ . The large uncertainties involved make it premature to implement  $(\text{H}_2\text{O})_2$  in GCMs. Further laboratory and *ab initio* studies of  $(\text{H}_2\text{O})_2$  properties are warranted.

Briegleb, B. P., 1992: Delta-eddington approximation for solar radiation in the NCAR community climate model. *J. Geophys. Res.*, **97**(D7), 7603–7612.

Chýlek, P., Q. Fu, H. C. W. Tso and D. J. W. Geldart, 1998: Contribution of water vapor dimers to clear sky absorption of solar radiation. *Submitted for publication*.

Chýlek, P. and D. J. W. Geldart, 1997: Water vapor dimers and atmospheric absorption of electromagnetic radiation. *Geophys. Res. Lett.*, **24**, 2015–2018.

Greenblatt, G. D., J. J. Orlando, J. B. Burkholder and A. R. Ravishankara, 1990: Absorption measurements of Oxygen between 330 and 1140 nm. *J. Geophys. Res.*, **95**(D11), 18577–18582.

Mlawer, E. J., S. A. Clough, P. D. Brown, T. M. Stephen, J. C. Landry, A. Goldman and F. J. Murcray, 1998: Observed atmospheric collision-induced absorption in near-infrared oxygen bands. *J. Geophys. Res.*, **103**(D4), 3859–3863.

Pfeilsticker, K., F. Erle and U. Platt, 1997: Absorption of solar radiation by atmospheric  $\text{O}_4$ . *J. Atmos. Sci.*, **54**(7), 933–939.

Solomon, S., R. W. Portmann, R. W. Sanders and J. S. Daniel, 1998: Absorption of solar radiation by water vapor, oxygen, and related collision pairs in the Earth’s atmosphere. *J. Geophys. Res.*, **103**(D4), 3847–3858.

Tso, H. C. W., J. W. Geldart and P. Chýlek, 1998: Anharmonicity and cross-section for absorption of radiation by water dimer. *In press in J. Chem. Phys.*

Zender, C. S., B. Bush, S. K. Pope, A. Bucholtz, W. D. Collins, J. T. Kiehl, F. P. J. Valero and J. Vitko, Jr., 1997: Atmospheric absorption during the Atmospheric Radiation Measurement (ARM) Enhanced Shortwave Experiment (ARESE). *J. Geophys. Res.*, **102**(D25), 29901–29915.